

Tight Integration of Feature-Based Relocalization in Monocular Direct Visual Odometry

Mariia Gladkova^{1,2}, Rui Wang^{1,2}, Niclas Zeller^{1,2}, and Daniel Cremers^{1,2}

Abstract—In this paper we propose a framework for integrating map-based relocalization into online direct visual odometry. To achieve map-based relocalization for direct methods, we integrate image features into Direct Sparse Odometry (DSO) and rely on feature matching to associate online visual odometry (VO) with a previously built map. The integration of the relocalization poses is threefold. Firstly, they are treated as pose priors and tightly integrated into the direct image alignment of the front-end tracking. Secondly, they are also tightly integrated into the back-end bundle adjustment. An online fusion module is further proposed to combine relative VO poses and global relocalization poses in a pose graph to estimate keyframe-wise smooth and globally accurate poses. We evaluate our method on two multi-weather datasets showing the benefits of integrating different handcrafted and learned features and demonstrating promising improvements on camera tracking accuracy.

Index Terms—SLAM, relocalization, map-based localization

I. INTRODUCTION

Visual odometry (VO) and simultaneous localization and mapping (SLAM) are important components of many autonomous systems that use cameras as one of their sensor modalities. For these systems, detection of a re-visited place can be crucial in correcting accumulated drift [1], recovering from tracking failure or solving the kidnapped robot problem [2]. These issues can be solved by camera *relocalization*, which is referred in this work as a process of continuous online estimation of 6DoF poses based on a pre-generated map. By continuously relocalizing we aim to extend the conventional use of relocalization as a recovery module [3], [4] and integrate its estimates into a visual odometry (VO) framework in a much more involved fashion.

Relocalization can be a challenging task due to significant differences between map and current visual data, possibly caused by weather and seasonal changes, as well as human activities like traffic and construction works. While feature-based VO and SLAM methods can tackle this problem by relying on repeatability and descriptiveness of local features, there is no straightforward way for direct methods to achieve relocalization. Usually sampled points are uniformly distributed across all image data and hold only pixel intensity values, which cannot guarantee any of the aforementioned feature qualities. Only limited efforts have been made to resolve such issue. In GN-Net [5], the raw images are replaced by learned feature maps to enhance the invariance to brightness changes. LDSO [6], on the other hand, proposes

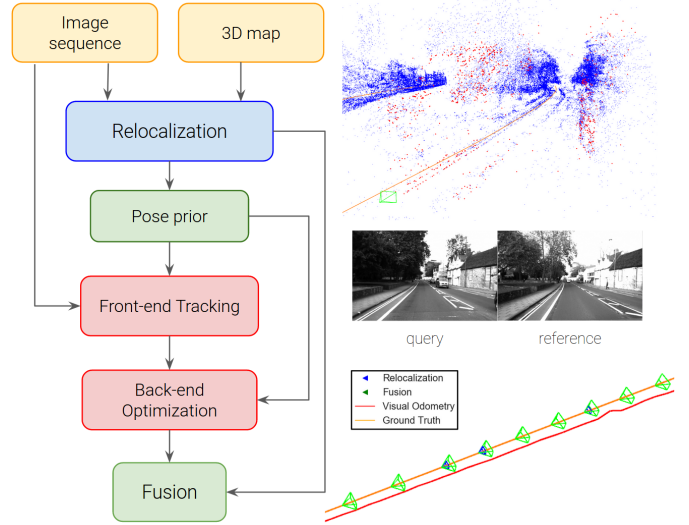


Fig. 1: Left: Proposed relocalization pipeline. The relocalization module consistently provides estimates of global camera poses against a pre-built map. Relocalization poses are tightly integrated into the front-end and back-end VO optimization framework to increase accuracy and robustness of camera tracking. Furthermore, the relative VO poses and global relocalization poses are fused in a pose graph optimization to obtain smooth and globally accurate poses. Top right: Overlay of the reference map (blue) with the VO point cloud (red) indicates that the estimated relocalization is accurate. Bottom right: The fused poses (green) closely follow the ground truth trajectory (orange line).

to integrate image features into DSO, thus combining the advantages of both families. In this work, we proceed in the direction of merging image features into direct methods. When a new frame arrives, in addition to tracking features with respect to a previous reference frame, we also track them against a pre-built map and a relocalization pose is obtained by feature matching. Relocalization poses are further utilized at three levels: by tightly integrating into the front-end tracking, by tightly integrating into the back-end bundle adjustment (BA), and by fusing with VO estimates to get a smooth and globally accurate trajectory. Tight integration of pose priors into a direct sparse odometry framework is inspired by D3VO work [7], where camera poses predicted by a deep network are utilized instead. Moreover, unlike LDSO [6] work, which considers only ORB features [8] for place recognition, feature tracking and matching, we integrate different handcrafted and learned features to unveil their pros and cons.

¹ Technical University of Munich

² Artisense GmbH

Contact: mariia.gladkova@tum.de

II. RELATED WORK

A. Indirect versus Direct VO / SLAM

Indirect VO / SLAM methods [9], [3], [4] have dominated the field for many years. Their success can be partially attributed to robust feature detectors and descriptors that incorporate invariance to geometric noise, brightness and viewpoint. An alternative, direct formulation, which skips abstraction into a feature space and directly works with pixel intensities, has been first proposed in [10] using an Extended Kalman Filter and then re-formulated as a non-linear optimization problem in [11], [12]. Direct methods sample interest points across an entire image space including edges and less-textured surfaces, which makes them generally more robust in cornerless environments. On the other hand, direct approaches are fragile to rapid motion and changes in illumination. Moreover, a good initialization is important to ensure optimization convergence and to guarantee an optimal solution. This makes direct methods inferior in wide-baseline matching, such as loop closure and relocalization, where global accuracy is desired. This issue is addressed in LDSO [6] work, where loop closure is achieved by adapting a point selection strategy and by introducing local features into a direct method.

B. Handcrafted and Learned Features

In recent years a number of computer vision tasks that require feature matching has significantly increased [13], [14], [3], [15]. These applications introduce different feature requirements such as computational efficiency, invariance to scale and affine transformation, robustness to noise and changes in lighting conditions. For many years SIFT [16] has been one of the most widely used feature descriptor, however its extraction is admitted to be computationally demanding [8]. Binary ORB features [8] that combine a FAST keypoint detector [17] and a BRIEF descriptor [18] have been proposed as an open-source, fast and lightweight alternative to SIFT. With the recent advances of deep learning, learned feature representations have shown a superior performance to handcrafted features [19]. Neural networks have been applied to separate tasks of keypoint localization [20], [21], descriptor learning [22], as well as to end-to-end feature extraction from images [23], [24]. In our work, we select three representative learned features, namely, SuperPoint [25], R2D2 [24] and ASLFeat [26]. They are integrated into a direct VO method and used to achieve map-based relocalization.

III. SYSTEM OVERVIEW

In the following sections we will describe the proposed SLAM and relocalization framework, as it is shown in Fig. 1, in detail. In general, our pipeline consists of three major modules: 1) a relocalization module, to obtain reference poses with respect to a pre-build map (Sec. V); 2) a VO module, which integrates the relocalization information to perform robust and accurate camera tracking within a local coordinate frame (Sec. IV); 3) a fusion module, which fuses map-based relocalization poses and visual odometry poses

to obtain a smooth and globally accurate camera trajectory (Sec. VI). While our VO module uses information from the relocalization module, it is also used to generate the map we are localizing against. Therefore, we will first describe our VO approach and afterwards proceed with the relocalization module. Finally, we will explain how both components are integrated in the fusion module.

IV. VISUAL ODOMETRY

Our VO module builds on top of DSO [12], a state-of-the-art direct visual odometry algorithm. For each new frame DSO estimates its initial pose with respect to a reference keyframe by direct image alignment. Poses of keyframes are then refined in a sliding window, where bundle adjustment jointly optimizes the points' depth and all keyframe poses by minimizing a corresponding photometric energy:

$$E_{\text{photo}} = \sum_{i \in \mathcal{F}} \sum_{\mathbf{p} \in \mathcal{P}_i} \sum_{j \in \text{obs}(\mathbf{p})} E_{\mathbf{p}j}, \quad (1)$$

where \mathcal{F} is a set of all keyframes, \mathcal{P}_i - a set of points hosted in a keyframe i , $\text{obs}(\mathbf{p})$ - a set of keyframes that observe a point \mathbf{p} . $E_{\mathbf{p}j}$ is a weighted photometric error term for a point \mathbf{p} hosted in a frame i and observed in a frame j . For details on the energy formulation please refer to [12].

A. Pose Priors

To improve the accuracy and robustness of VO, we use the information gained from relocalization against a pre-built map (Sec. V). The relocalization poses are used as priors for both the front-end tracking using the Coarse Tracker module [12] and the back-end bundle adjustment.

1) *Pose Prior for Coarse Tracker*: In the tracking front-end we use a relative pose prior $\hat{\mathbf{T}}_i^j \in \text{Sim}(3)$ obtained from relocalization, which transforms a 3D point from coordinate system of the last keyframe i to that of the current frame j . This prior is used as initialization for direct image alignment. Additionally, we construct a factor graph and impose pose prior based on relocalization as a binary factor between a reference keyframe and a current frame global poses. If pose prior $\hat{\mathbf{T}}_i^j$ is unavailable, the front-end is initialized based on a constant motion model, as described in [12].

2) *Pose Prior for Bundle Adjustment*: Keyframe poses optimized in the bundle adjustment are defined with respect to the common local coordinate frame. Therefore, one could think of lifting this common coordinate frame to a global frame based on the information obtained from relocalization and performing optimization of the global poses directly in the bundle adjustment. However, due to the marginalization of keyframes, this leads to numerical instabilities, especially in situations when relocalization poses are sparse or not available for the first frame. Hence, similar to the coarse tracker prior, we utilize relative pose priors between the keyframes respectively. We can derive a factor graph as shown in Fig. 2, where the red boxes refer to the photometric factors defined in Eq. (1), the green boxes refer to the marginalization factors. Relocalization factors (blue boxes)

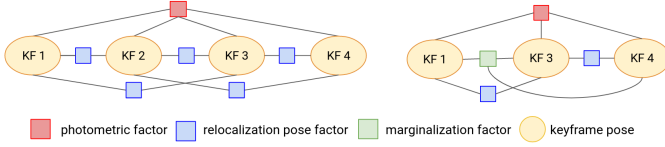


Fig. 2: Visualization of a factor graph created for the back-end optimization. Each relocalization factor represents a relative relocalization pose between corresponding keyframes. In case of marginalization (right), the residual energy is kept as a factor (green).

are imposed in the form of priors $\hat{\mathbf{T}}_i^j$ on the relative pose $\mathbf{T}_i^j \in \text{SE}(3)$ between keyframes i and j according to Eq. (2)

$$E_{\text{pose}} = \sum_{i \in \mathcal{F}} \sum_{\substack{j \in \mathcal{R}_i \\ j < i}} \text{Log}_{\text{SE}(3)}(\hat{\mathbf{T}}_j^i)^T \Sigma^{-1} \text{Log}_{\text{SE}(3)}(\hat{\mathbf{T}}_j^i), \quad (2)$$

where \mathcal{F} is a set of all keyframes, \mathcal{R}_i is a subset of \mathcal{F} , which includes keyframes that have a relocalization pose. In our work we limit $|\mathcal{R}_i| \leq 2$. When selecting keyframes for \mathcal{R}_i , the priority is given to the later ones, since the oldest keyframes can be shortly scheduled for marginalization. The inverse of a covariance matrix $\Sigma^{-1} \in \mathbb{R}^{6 \times 6}$ is modeled as a constant diagonal matrix and $\text{Log}_{\text{SE}(3)}(\cdot)$ is a mapping from an element of the Lie group $\text{SE}(3)$ to its twist coordinates in $\mathfrak{se}(3)$. For brevity and notation consistency we skip the transformations between elements of $\text{Sim}(3)$ and $\text{SE}(3)$ in the equations.

Combining photometric and relocalization factors, the total objective function becomes

$$E_{\text{total}} = E_{\text{photo}} + w E_{\text{pose}}, \quad (3)$$

where E_{photo} and E_{pose} are defined as in Eq. (1) and Eq. (2), respectively. This way pose prior can be regarded as a regularization term in the total optimized energy. The minimization of E_{total} is performed in a Gauss-Newton optimization scheme.

When a keyframe is scheduled for marginalization, we remove all its factors and add a factor corresponding to the residual energy after Schur complement. The visualization of the factor graph is shown in Fig. 2.

B. Feature Tracking

While photometric formulations show superior performance with respect to VO, they struggle in tasks like loop closure and relocalization, since in these cases a good initialization and photometric consistency cannot be guaranteed. Therefore, to be able to solve these problems we follow the idea of LDSO [6], which replaces a subset of the tracked and optimized points by keypoints with associate local descriptors. Since keypoints are tightly integrated into the photometric bundle adjustment, their accurate depth is estimated using the entire optimization window. While LDSO limits the use to handcrafted ORB features [8], we keep our pipeline more general, which enables integration of any local keypoint descriptors, including the learned ones.

The tracked features now can be used to solve tasks like loop closure to generate globally consistent maps or to perform relocalization against a pre-build map (Sec. V).

V. RELOCALIZATION

The relocalization module runs in parallel to the VO pipeline and finds tracking references for each frame. Relocalization is carried out in a two-stage approach. First, we find potential candidates in our map database using a Bag-of-Words (BoW) image retrieval model (Sec. V-A). Second, a relative pose between a current frame and its map-based reference is estimated from feature correspondences and a global relocalization pose is computed (Sec. V-B).

A. BoW Image Retrieval

After the system receives a new image, it extracts the local 2D features and converts them to a global descriptor using a BoW database.¹ Since such representation does not preserve the order of features in the image, it removes the spatial information from the feature layout and offers only a limited descriptive capability. To circumvent this problem we follow the *pyramid matching* method proposed in [28]. In particular, we switch to a multi-level representation of an image, that can be intuitively viewed as placing a grid of increasingly coarser resolution and aggregating the features in each grid cell for computing local histogram. We refer to Eq. (3) from [29] for further details of the underlying approach.

In our work, the histograms are computed based on the local keypoint descriptor assignments to visual words in a BoW codebook (process of quantization). To limit the number of images considered for similarity measure computation, we take advantage of the sequential nature of our queries and assume that the correct tracking references lie spatially close for consecutive frames.

B. Pose Refinement

We select 3 candidate images with the highest κ -values and proceed to feature matching. False correspondences are pruned using Lowe's ratio test [16] with threshold $\tau = 0.85$. Having 3D - 2D correspondences between a reference frame m and a current frame i we can estimate relative transformation $\mathbf{R}_m^i \in \text{SE}(3)$ using Perspective-n-Points (PnP) algorithm in a RANSAC scheme [30] and refine it by minimizing a geometric projection error. Final relocalization pose $\hat{\mathbf{T}}_i \in \text{Sim}(3)$ is computed by concatenating the respective relative transformation to the global pose of a map candidate that has the biggest number of feature correspondences.

VI. FUSION

In addition to integration of relocalization poses into direct image alignment and bundle adjustment we propose a local pose graph optimization that is intended to fuse odometry and relocalization estimations online. Since our relocalization module computes relative poses with respect to global map poses, they are suitable as pair-wise pose observations in a

¹For our implementation we use fbow library, a fast version of DBow2/DBow3 libraries [27].

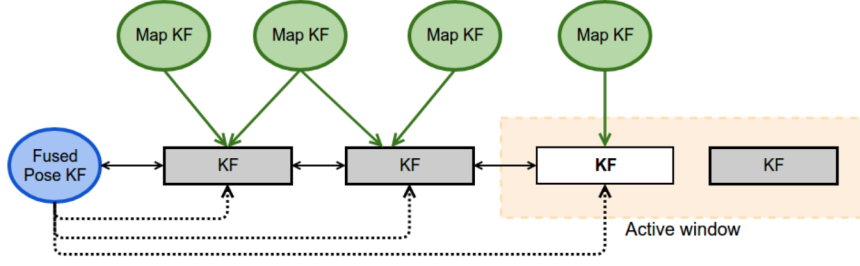


Fig. 3: Fusion pose graph visualization. Circular components represent fixed variables, whereas rectangular are subjects for optimization. Solid arrows show binary constraints, whereas dotted arrows represent initialization of variables. The direction of arrows depicts relative transformation between corresponding coordinate systems. The optimization objective lies in estimation of a fused pose for a keyframe in the white rectangle.

traditional pose graph framework. To ensure that our relative keyframe transformations are optimal, we base our pose graph on keyframes that lie outside the active optimization window.

The main objective of the local optimization lies in estimation of a fused pose $\mathbf{F}_k \in \text{Sim}(3)$ for keyframe k that has been recently finalized and scheduled for marginalization. To build the graph we consider only keyframes that appear earlier in the sequence and have a relocalization pose. After all keyframes are chosen, pose values are initialized based on the oldest inserted keyframe, which has already received a fused pose. Specifically, the initialization of estimated fused pose $\mathbf{F}_j \in \text{Sim}(3)$ is achieved by concatenating relative keyframe pose to fused pose \mathbf{F}_i of the reference keyframe i , i.e. $\mathbf{F}_j := \mathbf{T}_i^j \mathbf{F}_i$.

We distinguish two types of constraints, odometry-based $e_{i,j}$ and map-based $l_{i,j}$, which are defined in Eq. (4) and Eq. (5) respectively.

$$e_{i,j} := \text{Log}_{\text{Sim}(3)}(\mathbf{T}_j^i \mathbf{F}_i^j) \quad (4)$$

$$l_{i,j} := \text{Log}_{\text{Sim}(3)}((\hat{\mathbf{T}}_i \mathbf{M}_j^{-1})^{-1} \mathbf{F}_i \mathbf{M}_j^{-1}) \quad (5)$$

The total energy that is minimized in the local pose graph with N keyframes is represented by Eq. (6):

$$\begin{aligned} E_{\text{fusion}}^k &= w_1 E_{VO}^k + w_2 E_{MAP}^k \\ &= w_1 \sum_{i,j \in \mathcal{F}_k} e_{i,j}^T \Sigma^{-1} e_{i,j} + w_2 \sum_{i \in \mathcal{F}_k} \sum_{j \in \mathcal{L}_i} l_{i,j}^T \Lambda^{-1} l_{i,j}, \end{aligned} \quad (6)$$

where \mathcal{F}_k is a set of keyframes inserted into pose graph together with the keyframe k , \mathcal{L}_i is a set of tracking references for keyframe i . Lastly, $\Sigma^{-1}, \Lambda^{-1} \in \mathbb{R}^{7 \times 7}$ are inverses of covariance matrices, which are modeled as diagonal matrices. The visualization of the proposed pose graph can be seen in Fig. 3.

In our implementation, we take advantage of a possibility of having several tracking references per keyframe and impose at most 2 measurement constraints from the map. For optimizations we use Levenberg-Marquardt algorithm and fix all map poses together with the reference keyframe. Our implementation is based on g2o, an optimization library introduced in [31].

VII. EXPERIMENTS

We chose two different datasets to evaluate our method, namely the 4Seasons Dataset [32] and the Oxford RobotCar Dataset [33]. 4Seasons is a novel cross-season and multi-weather outdoor dataset created by traversing nine different environments multiple times. It provides accurate ground truth 6DoF camera poses with up-to centimeter precision. For our evaluations, we have selected one urban environment and used the sequences corresponding to six different traversals, which were captured in March and April of 2020. Since the sequences capture minor seasonal changes, we use them as a relatively less challenging setting. Oxford RobotCar is a challenging large-scale dataset which is created by traversing a single route in Oxford for over one year. It thus contains significantly different scene layouts, weather and seasonal conditions. For a more challenging setting for our evaluation, we have chosen 3 sequences: 2014-11-18-13-20 (cloudy), 2014-12-09-13-21 (overcast) and 2015-08-12-15-04 (sunny) and used the provided Real-time Kinematic (RTK) poses [34] as ground truth.

A. Integrating Pose Prior to Visual Odometry

To verify the benefits of integrating pose priors based on the relocalization module (Sec. IV-A) into a VO system, we conduct thorough experiments on the chosen datasets. For each dataset, we create sequence pairs among the selected sequences. One sequence from every pair is used for running VO, whereas the other is deployed for generating the map. Three settings are evaluated for each sequence pair, namely “no prior” (i.e. conventional VO), “prior in the front-end tracking” and “prior in both the front-end tracking and the back-end BA”. In addition, we evaluate the influence of integrating different feature types into the direct method, namely a handcrafted feature, ORB [8], and three learned features, SuperPoint [25], ASLFeat [26] and R2D2 [24]. The relative pose error (RPE) [35] is adopted for quantification. As pointed out by [35], rotational errors appear as translational errors when a camera moves, we therefore only consider the translational error in meters. The relative errors are computed by using an interval of 7 keyframes.

The results on 4Seasons sequences are shown in Table I, where the rows are grouped and arranged according to increased difficulties. Note that the first row corresponds to

Configuration	Odometry / Map	no prior / prior in front-end / prior in front-end and back-end			
		ORB	SuperPoint	ASLFeat	R2D2
same sequence	03-24.17-36-22 / 03-24.17-36-22	0.31 / 0.20 / 0.11	0.36 / 0.09 / 0.09	0.11 / 0.16 / 0.15	1.40 / 0.18 / 0.17
shadows / shadows	03-24.17-36-22 / 03-24.17-45-37	0.39 / 0.40 / 0.19	0.36 / 0.13 / 0.09	0.11 / 0.19 / 0.15	1.61 / 0.20 / 0.18
sunny / sunny	04-07.10-35-45 / 04-07.10-20-32	0.42 / 0.23 / 0.19	0.48 / 0.32 / 0.17	0.49 / 0.24 / 0.15	1.22 / 0.47 / 0.42
sunny / shadows	04-07.10-35-45 / 03-24.17-36-22	0.39 / 0.25 / 0.59	0.40 / 0.32 / 0.26	0.67 / 0.41 / 0.26	1.46 / 0.71 / 0.86
shadows / overcast	03-24.17-36-22 / 03-03.11-52-19	0.59 / 0.39 / 0.37	0.41 / 0.15 / 0.13	0.15 / 0.35 / 0.29	1.35 / 0.65 / 0.53
sunny / foliage	04-07.10-35-45 / 04-23.19-37-00	0.40 / 0.35 / 0.64	0.40 / 0.30 / 0.37	0.69 / 0.50 / 0.54	1.45 / 1.34 / 1.44

TABLE I: Relative Pose Error (RPE) on 4Seasons sequences. Each column shows the results of integrating different features into the direct method. The values are expressed in meters and computed with an interval of 7 keyframes. The best results are shown in bold and underlined.

Configuration	Odometry / Map	no prior / prior in front-end / prior in front-end and back-end			
		ORB	SuperPoint	ASLFeat	R2D2
same sequence	2014-12-09-13-21-02 / 2014-12-09-13-21-02	0.11 / 0.10 / 0.10	0.13 / 0.11 / 0.10	0.89 / 0.26 / 0.15	0.29 / 0.10 / 0.11
cloudy / overcast	2014-11-18-13-20-12 / 2014-12-09-13-21-02	0.27 / 0.22 / 0.23	0.38 / 0.24 / 0.15	0.96 / 0.23 / 0.16	0.74 / 0.17 / 0.16
cloudy / sunny	2014-11-18-13-20-12 / 2015-08-12-15-04-18	0.28 / 0.32 / 0.35	0.35 / 0.20 / 0.16	1.08 / 0.32 / 0.17	0.73 / 0.58 / 0.49
overcast / cloudy	2014-12-09-13-21-02 / 2014-11-18-13-20-12	0.12 / 0.10 / 0.11	0.12 / 0.14 / 0.17	0.83 / 0.23 / 0.15	0.25 / 0.15 / 0.17
overcast / sunny	2014-12-09-13-21-02 / 2015-08-12-15-04-18	0.11 / 0.12 / 0.13	0.11 / 0.14 / 0.16	0.84 / 0.23 / 0.13	0.24 / 0.16 / 0.23
sunny / cloudy	2015-08-12-15-04-18 / 2014-11-18-13-20-12	0.12 / 0.15 / 0.22	0.11 / 0.12 / 0.13	0.29 / 0.15 / 0.12	0.42 / 0.29 / 0.37
sunny / overcast	2015-08-12-15-04-18 / 2014-12-09-13-21-02	0.12 / 0.15 / 0.13	0.12 / 0.14 / 0.15	0.27 / 0.20 / 0.15	0.38 / 0.18 / 0.14

TABLE II: Relative Pose Error (RPE) on Oxford RobotCar sequences. Each column shows the results of integrating different features into the direct method. The values are expressed in meters and computed with an interval of 7 keyframes. The best results are shown in bold and underlined.

the case of using the same sequence for map and VO, which is an idealistic scenario and shown as a reference. As it can be seen from the table, pose prior based on relocalization poses generally improves camera tracking. Some notable exceptions appear with ASLFeat for the sequences with shadows, where relocalization accuracy is not sufficient to boost pure odometry results.

Three sequences with different weathers and seasonal conditions are selected from Oxford RobotCar dataset to further increase the distinctions between the VO and map sequences. The results are presented in Table II. As now the corresponding images from the map and VO sequences often look significantly different, the performance of matching ORB and SuperPoint features starts to degrade, thus integration of pose priors does not improve when compared to the pure VO mode. It should be noted, though, that despite underperforming feature matching, our integration maintains the system stability and does not significantly worsen the VO performance. On the other hand, in these more challenging conditions, relocalization based on more advanced features like ASLFeat and R2D2 helps to improve over pure VO, as shown in the last two columns.

B. Map-Based Relocalization and Fusion with Visual Odometry

In this section, we verify quality of relocalization poses and benefit of fusing them with the VO results. As explained in Section VI, by fusing the VO results with the relocalization poses, our method can estimate the global poses defined in the reference coordinate system of the map. This makes it meaningful to evaluate the global pose errors. In all the following experiments, the absolute trajectory error (ATE) [35] (in meters) is used.

On 4Seasons dataset we select three sequence pairs with increasingly challenging configurations on weather and seasonal conditions, namely “shadows / shadows”, “shadows /

overcast” and “sunny-foliage”. The two features that work dedicatedly on grayscale images are evaluated, namely ORB and SuperPoint. The cumulative error plots together with some example images from odometry and map sequences are shown in Fig. 4. It is apparent that fusing the relocalization poses with the VO results consistently improves pose accuracy. It is worth noting that the relocalization curves often saturate to values less than 100%, which means we do not get relocalization poses for all the frames. Yet our fusion unquestionably boosts the performances in those cases. Due to the significant differences caused by seasonal change, relocalization based on ORB features is unsuccessful for the majority of keyframes in the configuration of “sunny-foliage”. Therefore, fusion estimates are not globally accurate in this case.

We further verify our relocalization and fusion on Oxford RobotCar dataset, using the same sequence pairs as in the previous section. All the four selected features are tested and the cumulative absolute translational errors are shown in Fig. 5. Despite the much more challenging configurations compared to the 4Seasons experiments, our fusion consistently improves the performances over relocalization for all the tested features. It is worth noting that we do not show the results of pure VO in these plots, as monocular VO methods typically have much larger absolute errors than the limit used in the plots.

Lastly, we compare our results to several popular monocular and stereo VO / SLAM methods, including ORB-SLAM2 [36] (monocular / stereo, VO / SLAM), DSO [12], LDSO [6] (VO / SLAM) and Stereo DSO [37]. The results are shown in Table III. The experiments are conducted on a sequence with shadows from the 4Seasons dataset. Our approach is evaluated with two map sequences, namely (a) shadows and (b) overcast. From the table it can be seen that our method outperform all other VO and SLAM systems.

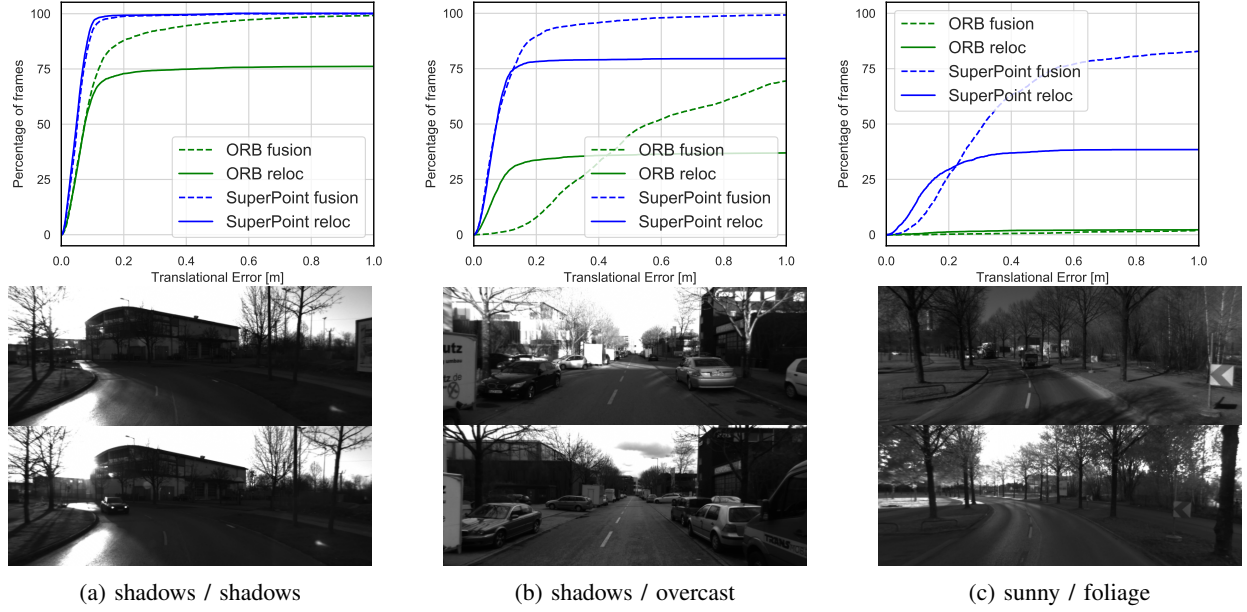


Fig. 4: Cumulative Absolute Translational Error on 4Seasons sequences. Fusing the relocalization poses with VO results in a pose graph consistently improves the performances. Note that relocalization based on ORB does not work for “sunny-foliage” due to low relocalization success rate caused by seasonal change (relocalization availability $\approx 2\%$).

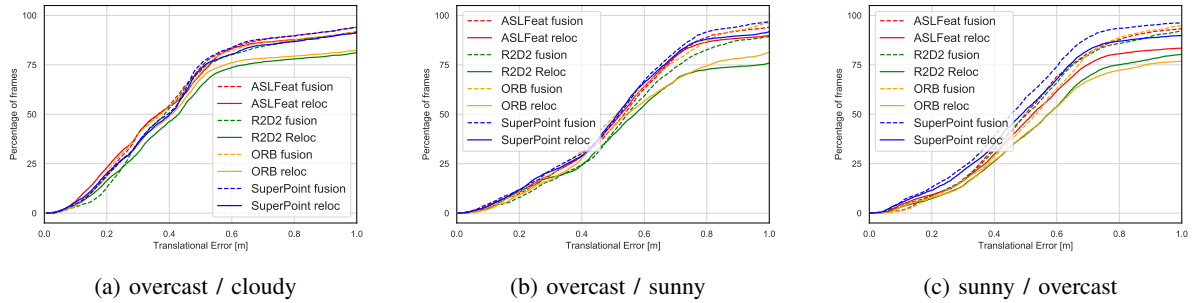


Fig. 5: Cumulative Absolute Translational Error on Oxford RobotCar sequences. Fusing the relocalization poses with VO results in a pose graph consistently improves the performances.

With respect to the absolute error this result is anticipated, since we are localizing against a globally accurate map. However, also with respect to RPE our method performs better than all monocular approaches and shows on par results with stereo methods, including state-of-the-art direct and indirect systems. This indicates that our fusion outputs are both globally and locally accurate.

VIII. CONCLUSION

In this paper we present a complete framework which combines direct VO and feature-based relocalization. We extensively evaluate our approach on two multi-weather datasets. Our experiments show that by integrating pose priors obtained from relocalization into both the front-end tracking and the back-end optimization of a direct VO method, we can significantly improve the tracking accuracy. We also show that the proposed fusion module is able to estimate globally accurate poses, even when relocalization is not successful for every frame. Furthermore, using our

Mono / Stereo	Method	ATE [m]	RPE [m]
M	Fusion ^a	0.11	0.03
M	Fusion ^b	0.22	0.07
M	ORB-SLAM2 VO	147.90	29.49
M	ORB-SLAM2 SLAM	14.52	0.16
M	DSO	17.30	0.11
M	LDSO SLAM	37.42	0.53
M	LDSO VO	138.69	10.27
S	ORB-SLAM2 VO	5.98	0.04
S	ORB-SLAM2 SLAM	1.32	0.03
S	Stereo DSO	1.64	0.02

TABLE III: Comparison to VO / SLAM on 4Seasons sequence with shadows. RPE is evaluated per traveled meter. The best and the second best values are shown in bold, the former is also underlined. Fusion is reported for (a) shadows, (b) overcast map sequence using SuperPoint features.

pipeline we investigate the strength of different feature types. We hope that our work has revealed the power of combining the strengths of both direct and indirect approaches in the context of SLAM and that it will drive further research in this direction.

REFERENCES

- [1] C. Cadena, L. Carlone, H. Carrillo, Y. Latif, D. Scaramuzza, J. Neira, I. Reid, and J. J. Leonard, "Past, present, and future of simultaneous localization and mapping: Toward the robust-perception age," *IEEE Transactions on robotics*, vol. 32, no. 6, pp. 1309–1332, 2016.
- [2] J. Fuentes-Pacheco, J. Ruiz-Ascencio, and J. M. Rendón-Mancha, "Visual simultaneous localization and mapping: a survey," *Artificial intelligence review*, vol. 43, no. 1, pp. 55–81, 2015.
- [3] G. Klein and D. Murray, "Parallel tracking and mapping for small ar workspaces," in *2007 6th IEEE and ACM international symposium on mixed and augmented reality*, pp. 225–234, IEEE, 2007.
- [4] R. Mur-Artal, J. M. M. Montiel, and J. D. Tardos, "Orb-slam: a versatile and accurate monocular slam system," *IEEE transactions on robotics*, vol. 31, no. 5, pp. 1147–1163, 2015.
- [5] L. von Stumberg, P. Wenzel, Q. Khan, and D. Cremers, "Gn-net: The gauss-newton loss for multi-weather relocalization," *IEEE Robotics and Automation Letters*, vol. 5, no. 2, pp. 890–897, 2020.
- [6] X. Gao, R. Wang, N. Demmel, and D. Cremers, "Ldso: Direct sparse odometry with loop closure," in *2018 IEEE/RSJ International Conference on Intelligent Robots and Systems (IROS)*, pp. 2198–2204, IEEE, 2018.
- [7] N. Yang, L. v. Stumberg, R. Wang, and D. Cremers, "D3vo: Deep depth, deep pose and deep uncertainty for monocular visual odometry," in *Proceedings of the IEEE/CVF Conference on Computer Vision and Pattern Recognition*, pp. 1281–1292, 2020.
- [8] E. Rublee, V. Rabaud, K. Konolige, and G. Bradski, "Orb: An efficient alternative to sift or surf," in *2011 International conference on computer vision*, pp. 2564–2571, 2011.
- [9] A. J. Davison, I. D. Reid, N. D. Molton, and O. Stasse, "Monoslam: Real-time single camera slam," *IEEE transactions on pattern analysis and machine intelligence*, vol. 29, no. 6, pp. 1052–1067, 2007.
- [10] H. Jin, P. Favaro, and S. Soatto, "A semi-direct approach to structure from motion," *The Visual Computer*, vol. 19, no. 6, pp. 377–394, 2003.
- [11] J. Engel, T. Schöps, and D. Cremers, "Lsd-slam: Large-scale direct monocular slam," in *European conference on computer vision*, pp. 834–849, Springer, 2014.
- [12] J. Engel, V. Koltun, and D. Cremers, "Direct sparse odometry," *IEEE transactions on pattern analysis and machine intelligence*, vol. 40, no. 3, pp. 611–625, 2017.
- [13] S. Agarwal, Y. Furukawa, N. Snavely, I. Simon, B. Curless, S. M. Seitz, and R. Szeliski, "Building rome in a day," *Communications of the ACM*, vol. 54, no. 10, pp. 105–112, 2011.
- [14] T. Sattler, B. Leibe, and L. Kobbelt, "Fast image-based localization using direct 2d-to-3d matching," in *2011 International Conference on Computer Vision*, pp. 667–674, IEEE, 2011.
- [15] J. L. Schönberger, T. Price, T. Sattler, J.-M. Frahm, and M. Pollefeys, "A vote-and-verify strategy for fast spatial verification in image retrieval," in *Asian Conference on Computer Vision*, pp. 321–337, Springer, 2016.
- [16] D. G. Lowe, "Distinctive image features from scale-invariant keypoints," *International journal of computer vision*, vol. 60, no. 2, pp. 91–110, 2004.
- [17] E. Rosten and T. Drummond, "Machine learning for high-speed corner detection," in *European conference on computer vision*, pp. 430–443, Springer, 2006.
- [18] M. Calonder, V. Lepetit, C. Strecha, and P. Fua, "Brief: Binary robust independent elementary features," in *European conference on computer vision*, pp. 778–792, Springer, 2010.
- [19] J. L. Schönberger, H. Hardmeier, T. Sattler, and M. Pollefeys, "Comparative evaluation of hand-crafted and learned local features," in *Proceedings of the IEEE Conference on Computer Vision and Pattern Recognition*, pp. 1482–1491, 2017.
- [20] S. Huang, M. Gong, and D. Tao, "A coarse-fine network for keypoint localization," in *Proceedings of the IEEE International Conference on Computer Vision*, pp. 3028–3037, 2017.
- [21] S. Suwajanakorn, N. Snavely, J. J. Tompson, and M. Norouzi, "Discovery of latent 3d keypoints via end-to-end geometric reasoning," in *Advances in neural information processing systems*, pp. 2059–2070, 2018.
- [22] V. Balntas, E. Riba, D. Ponsa, and K. Mikolajczyk, "Learning local feature descriptors with triplets and shallow convolutional neural networks," in *Bmvc*, 2016.
- [23] K. M. Yi, E. Trulls, V. Lepetit, and P. Fua, "Lift: Learned invariant feature transform," in *European Conference on Computer Vision*, pp. 467–483, Springer, 2016.
- [24] J. Revaud, C. De Souza, M. Humenberger, and P. Weinzaepfel, "R2d2: Reliable and repeatable detector and descriptor," in *Advances in Neural Information Processing Systems*, pp. 12405–12415, 2019.
- [25] D. DeTone, T. Malisiewicz, and A. Rabinovich, "Superpoint: Self-supervised interest point detection and description," in *Proceedings of the IEEE Conference on Computer Vision and Pattern Recognition Workshops*, pp. 224–236, 2018.
- [26] Z. Luo, L. Zhou, X. Bai, H. Chen, J. Zhang, Y. Yao, S. Li, T. Fang, and L. Quan, "Aslfeat: Learning local features of accurate shape and localization," in *Proceedings of the IEEE/CVF Conference on Computer Vision and Pattern Recognition*, pp. 6589–6598, 2020.
- [27] D. Gálvez-López and J. D. Tardós, "Bags of binary words for fast place recognition in image sequences," *IEEE Transactions on Robotics*, vol. 28, pp. 1188–1197, October 2012.
- [28] K. Grauman and T. Darrell, "The pyramid match kernel: Discriminative classification with sets of image features," in *Tenth IEEE International Conference on Computer Vision (ICCV'05) Volume 1*, vol. 2, pp. 1458–1465, IEEE, 2005.
- [29] S. Lazebnik, C. Schmid, and J. Ponce, "Beyond bags of features: Spatial pyramid matching for recognizing natural scene categories," in *2006 IEEE Computer Society Conference on Computer Vision and Pattern Recognition (CVPR'06)*, vol. 2, pp. 2169–2178, IEEE, 2006.
- [30] M. A. Fischler and R. C. Bolles, "Random sample consensus: a paradigm for model fitting with applications to image analysis and automated cartography," *Communications of the ACM*, vol. 24, no. 6, pp. 381–395, 1981.
- [31] G. Grisetti, R. Kümmerle, H. Strasdat, and K. Konolige, "g2o: A general framework for (hyper) graph optimization," in *Proceedings of the IEEE International Conference on Robotics and Automation (ICRA)*, Shanghai, China, pp. 9–13, 2011.
- [32] P. Wenzel, R. Wang, N. Yang, Q. Cheng, Q. Khan, L. von Stumberg, N. Zeller, and D. Cremers, "4seasons: A cross-season dataset for multi-weather slam in autonomous driving," *arXiv preprint arXiv:2009.06364*, 2020.
- [33] W. Maddern, G. Pascoe, C. Linegar, and P. Newman, "1 year, 1000 km: The oxford robotcar dataset," *The International Journal of Robotics Research*, vol. 36, no. 1, pp. 3–15, 2017.
- [34] W. Maddern, G. Pascoe, M. Gadd, D. Barnes, B. Yeomans, and P. Newman, "Real-time kinematic ground truth for the oxford robotcar dataset," *arXiv preprint arXiv:2002.10152*, 2020.
- [35] J. Sturm, N. Engelhard, F. Endres, W. Burgard, and D. Cremers, "A benchmark for the evaluation of rgb-d slam systems," in *2012 IEEE/RSJ International Conference on Intelligent Robots and Systems*, pp. 573–580, IEEE, 2012.
- [36] R. Mur-Artal and J. D. Tardós, "ORB-SLAM2: an open-source SLAM system for monocular, stereo and RGB-D cameras," *IEEE Transactions on Robotics*, vol. 33, no. 5, pp. 1255–1262, 2017.
- [37] R. Wang, M. Schworer, and D. Cremers, "Stereo DSO: Large-scale direct sparse visual odometry with stereo cameras," in *Proceedings of the IEEE International Conference on Computer Vision*, pp. 3903–3911, 2017.